Imaging at Radio through Submillimeter Wavelengths
ASP Conference Series, Vol. 3×10^8*, 2000*
J. G. Mangum and S. J. E. Radford, eds.

Amplitude Calibration in Interferometry

W. J. Welch, D. C.-J. Bock, M. C. Fleming, & D. D. Thornton

Radio Astronomy Laboratory, University of California, Berkeley, CA 94720. Email: dbock, welch, fleming, thornton@astro.berkeley.edu

Abstract.
This paper describes a novel two temperature amplitude calibration scheme for radio-astronomical antennas. Each of two temperature-regulated loads can be weakly coupled to the radiometer through a small hole in the antenna secondary mirror. Switching between the loads with a rapidly moving mirror provides a small difference signal at the radiometer input. The signal is broadband and stable. We have built and tested a prototype on one antenna in the BIMA Array, obtaining a calibration accuracy of better than one percent. Using this technique, one must separately measure the attenuation of the atmosphere using an antenna tipping measurement. Tests show that the tipping measurement provides attenuation calibration with an accuracy of 1%.

1. Introduction

Amplitude calibration is as important for interferometry as it is for single dish observing. Accurate amplitude scales are essential for the comparison of images made with different instruments. For example, the measurement of spectral indices in continuum emission processes is badly compromised by poor amplitude calibration. Good calibration is especially important when combining single dish and interferometer data, since there may be only a small overlap in spatial frequency coverage. For optimum fidelity, good calibration among the different antennas of an array is also important, especially when self-calibration is not possible.

The technique presently used at most millimeter telescopes is the *chopper wheel method* introduced by Penzias & Burrus (1973), in which an observed source is compared with the difference between the sky brightness and an ambient temperature load. The physical temperature of the absorbing atmosphere is approximately the same as the ambient load and a mean model of the atmosphere is used to make a correction. The method is convenient, and absolute accuracies of a few percent are often obtained. One important advantage of this method is that the attenuation of the atmosphere is taken into account in the calibration and no separate measurement of extinction is needed. On days that have an uneven atmosphere, perhaps due to partial cloud cover, one still gets an approximate amplitude calibration. However, the approximation that the physical temperature of the air is the same as that of the ambient absorber is a significant source of error. Obtaining calibration accuracies at the level of 1% or better requires the use of two well-characterized black-body loads.

2. Correction for Extinction

Unlike the chopper wheel method, which provides a calibration with atmospheric extinction automatically taken into account, the present scheme requires a separate measurement of the extinction. Consider the input to the receiver:

$$T_{\rm in}(z) = T_0\alpha(z) + T_{\rm rcvr} + T_{\rm bb}e^{-\tau_0 \sec z} + \langle T_{\rm air}\rangle \left(1 - e^{-\tau_0 \sec z}\right), \tag{1}$$

with the antenna temperature $T_0\alpha(z)$, weakly dependent on the zenith distance z; the receiver temperature $T_{\rm rcvr}$; the contribution of the 3 K background radiation $T_{\rm bb}$; the zenith opacity τ_0; and the mean air temperature $\langle T_{\rm air}\rangle$. In good weather it is possible to determine $T_{\rm rcvr}$ and τ_0 from *tipping curves*—measurements of $T_{\rm in}(z)$ over a range of z (§4.3.).

This measurement of opacity depends on the uncertainty in the air temperature. The sensitivity to this uncertainty is less than it is for the chopper wheel method, but the uncertainty is still an important concern. The approximate error in τ_0 may be written as

$$\delta\tau_0 = \sqrt{\left(\frac{\epsilon}{\langle T_{\rm air}\rangle \sec z}\right)^2 + \left(\frac{\delta \langle T_{air}\rangle \tau_0}{\langle T_{\rm air}\rangle}\right)^2} \tag{2}$$

where ϵ is the error in the fit. For typical values: $\langle T_{\rm air}\rangle = 280$ K, $\delta \langle T_{\rm air}\rangle = 10$ K, $\tau_0 = 0.2$, $\sec z = 1.5$, and $\epsilon = 0.5$, we have $\delta\tau_0 = 0.0072$ and thus $e^{\delta\tau_0 \sec z} = 1.011$, so the error is about 1%.

When the atmosphere is not stable enough for reliable tipping measurements, the new hardware can be used in an enhanced chopper wheel method. The mirror which presents in turn the loads to the receiver has a third position which presents a concave scattering mirror, reflecting the sky. This may then be compared with the antenna temperature when the ambient load is presented. The advantages above the usual chopper wheel method are that the ambient load will have well-known temperature, and that the measurement will be continuous and small, avoiding non-linearities in the receiving system.

3. System Implementation

3.1. Optics

The principal hardware for the system is located behind the Cassegrain secondary mirror and is viewed through a 6 cm diameter hole, which corresponds to the image of the vertex window in the aperture plane. Immediately behind the hole (Figure 1) is a rotating 45° mirror which couples in one of the two calibration loads (at approximately 310 K and 400 K) or the scattering mirror. The rotating mirror has very low rotational inertia, allowing it to be rotated 90° in just 50 ms. Vibrations in the system have been minimized by matching and cancelling the moment of inertia of the stepping motor with that of the mirror. The

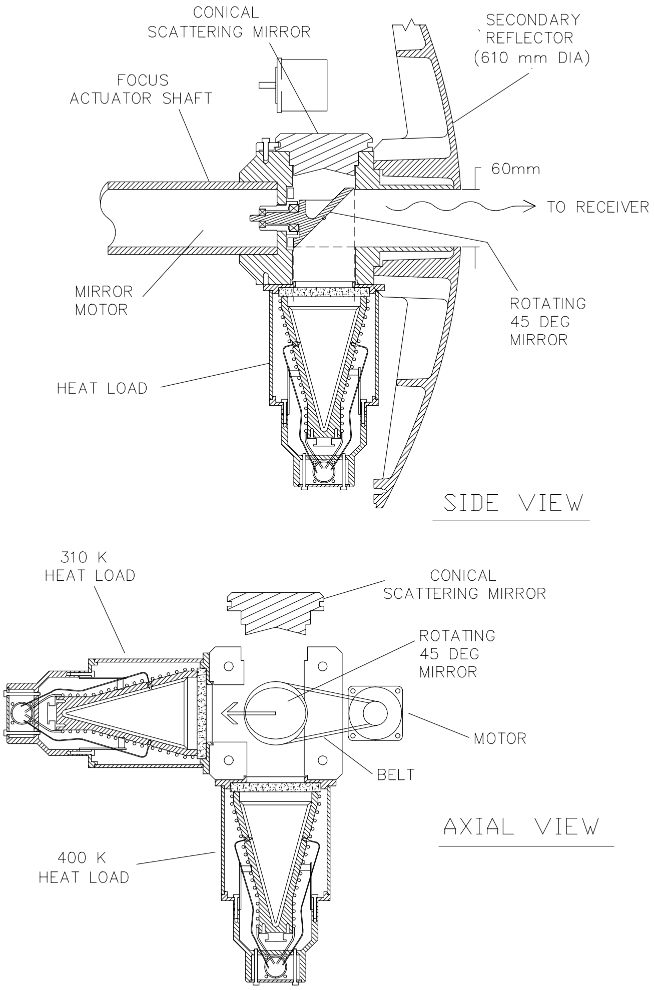

Figure 1. Sectional view of the subreflector assembly.

concave conical scattering mirror has an opening angle of 169° to reflect the sky while minimizing vignetting (Figure 2). At millimeter wavelengths the system is quasi-optical. However, the optical path behind the subreflector is confined to an over-moded waveguide to minimize coupling to ambient. A photograph of components of the system is in Figure 3.

3.2. Temperature Controlled Loads

Each of the two identical calibration loads (Figure 4) consists of a silicone-based absorber inside a well-insulated housing. The absorber has been cast onto a thick aluminum substrate which is wrapped in a rope heater. The heater is driven by a control circuit which regulates the substrate to better than 0.1 K. The uncertainty in the physical temperature of the load has two parts. The first part is a temperature drop across the absorber due to heat flow from the

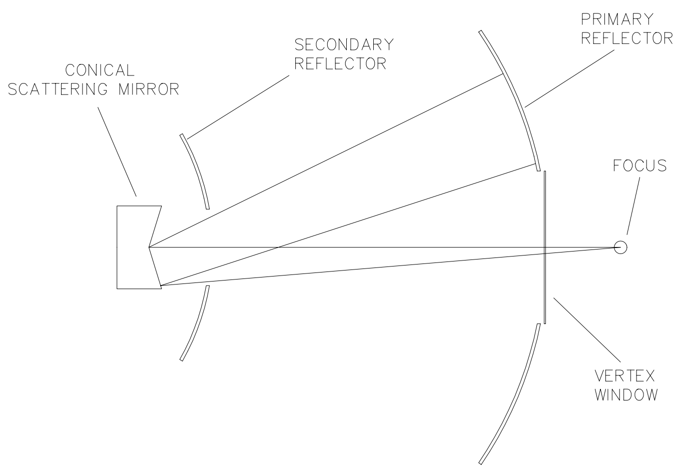

Figure 2. Cassegrain optics, showing how the scattering mirror takes the role of the conventional subreflector scattering cone, reflecting the sky to the receiver and thus preventing the return of axial rays.

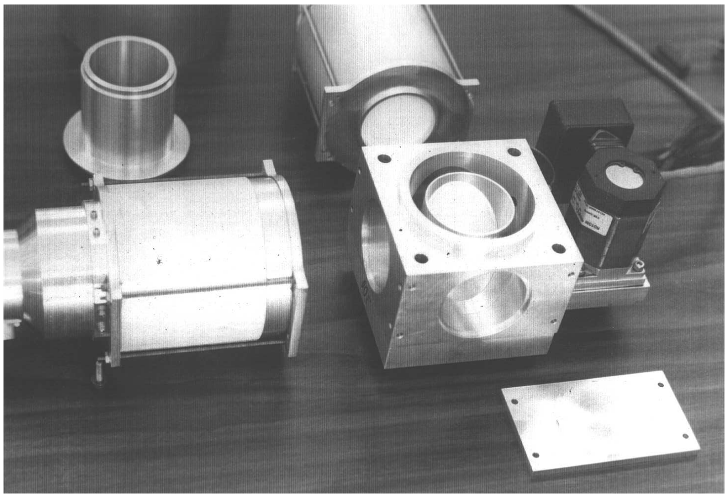

Figure 3. Photograph of the hardware located behind the subreflector, showing the rotating mirror, the temperature-controlled loads and the conical scattering mirror.

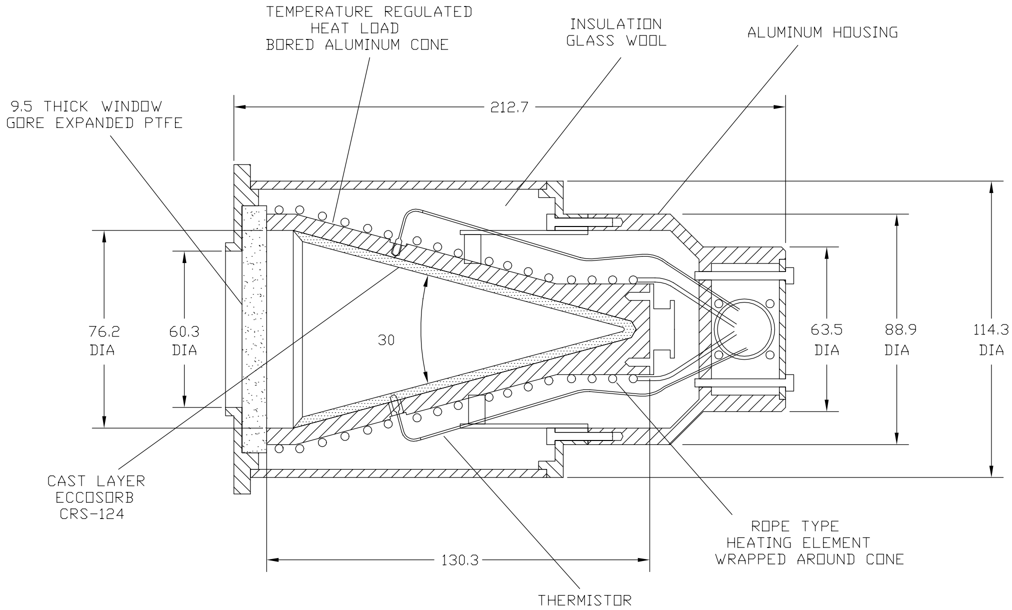

Figure 4. Diagram of one temperature-controlled load. Dimensions in mm.

ambient-temperature surroundings (since the absorber is not a perfect conductor). The magnitude of this effect is about 0.5 K for the 310 K load and 0.1 K for the 400 K load (for which the regulator servo has a higher gain). After corrections based on the ambient temperature, the uncertainty due to this effect and to regulation errors is 0.1 K, about 0.1% of the calibration signal difference. The second error is because we measure the absorber temperature at only one typical location. Laboratory measurements at several positions showed that this uncertainty is less than 0.5°; in any case it becomes a constant within the radiometrically measured load coupling coefficient (section 4.1.). The cone opening angle (30°) is close to the Brewster angle, so one polarization of an incident ray is absorbed. The other polarization undergoes at least 5 reflections within the cone, ensuring significant attenuation. Thus the cone is essentially a blackbody with radiometric temperature equal to its physical temperature.

3.3. Control and Data Acquisition

The rotating mirror is synchronized with the fundamental 320 ms control and data cycle of the array. Since the stepping motor provides a consistent drive time, the time for which the mirror is stationary and presenting a given load is reproducible. The output of a square-law detector at the receiver is integrated separately during the on-source time for each load. Eventually this data acquisition will take place in the correlator, providing a spectral-line calibration of the entire receiver system.

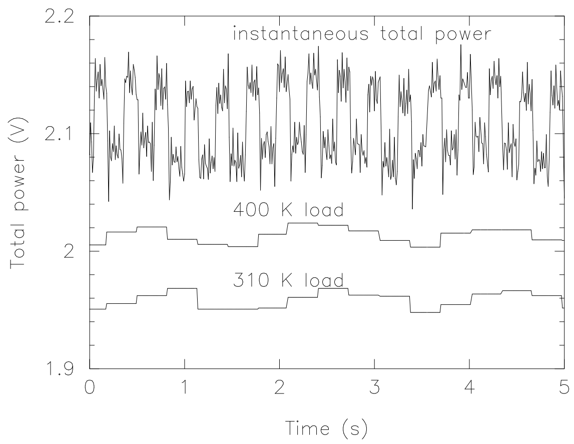

Figure 5. Total power detection of the calibration loads.

4. Test Results

4.1. Primary Calibration

We require a primary calibration of the difference signal coupling to the radiometer. An approximate calculation, based on the feed illumination of the subreflector, shows that the coupling of the hole is about 2%, corresponding to a temperature difference of about 1.8 K. For the primary calibration of this signal, an ambient load and one in boiling liquid nitrogen (LN) are the standards. The latter is in a radio-transparent foam box. The dielectric constant of the LN is 1.2, leading to a reflection of 1% at the interface between the foam box and the LN. This raises the effective LN blackbody temperature by $0.01(T_{amb} - T_{LN}) = 2.1$ K, and we estimate the error in making this correction to be 0.5 K. The ambient load is on a wheel in front of the receiver in the vertex cabin and its temperature is measured to an accuracy of about 0.5 K. The quadrature sum of these errors is 0.7 K, or about 0.35% of the difference between the ambient and LN loads. The calibration procedure consists of measuring in turn the rapidly chopped signal from the loads in the secondary mirror and the sequence of the LN and ambient loads completely covering the receiver beam. A calibration at 225 GHz gave a chopped signal of 1.77% (1.58 K).

4.2. Calibration Signal

Figure 5 shows the chopped signal from the secondary with a switching rate of 3 Hz. The periodic variation in the temperatures, seen best in the averages at the bottom of the figure, results from temperature cycling in the 4 K Gifford-McMahon refrigerator. The period of the chop is a sub-multiple of the refrigerator cycle so that the cycle is sampled without aliasing.

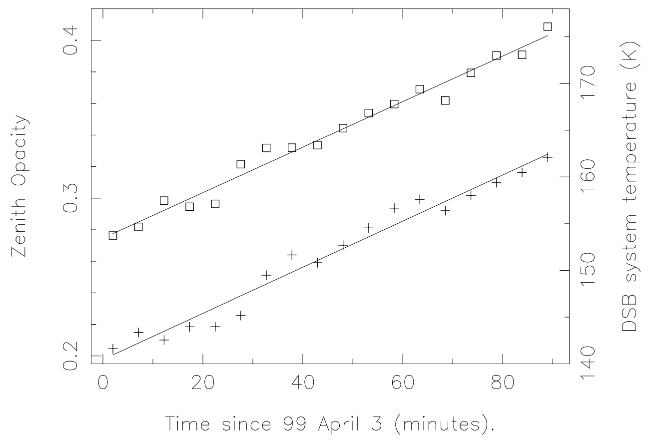

Figure 6. Variation with time of opacity (boxes) and brightness temperature at 60° elevation (crosses).

4.3. Tipping Curves

A series of tipping curve observations at 225 GHz was made over a two-hour interval in clear and calm weather. The derived opacities, shown in Figure 6, show a monotonic increase in time. A least squares line is drawn through the results. The scatter in the opacities about the line gives a conservative measure of the uncertainties in the measurement, since part of the deviation could represent non-linear changes in opacity. The RMS of the scatter about the line is σ_T=.0037. The effect of this error at 30° elevation is $e^{\sigma_T \sec 60^\circ} = 1.007$, a little less than 1%.

An estimate of the uncertainty of sky brightness measurements follows from a series of measurements at the same elevation, 60°, throughout the run of tipping measurements. Figure 6 shows these measurements with a straight line fit to the data. The RMS of the deviation from this straight line provides a conservative measure of the uncertainty of the measurements, since part of the deviation could represent real changes in the brightness. This measure of the scatter is 1.2 K, which is 0.8%.

The intercept of each tipping curve measures the sum of the receiver and antenna temperatures (Figure 7). There is no systematic difference between the intercepts, supporting the model of monotonically changing extinction. The receiver temperature was determined separately from the LN and ambient load measurements to be 63 K. The average of the intercepts is 75 K, implying an antenna temperature of 12 K, consistent with the known 100 GHz value of 7 K, assuming that the temperature is due largely to losses in the metal reflectors.

4.4. Accuracy of Single Calibrations

Apart from the primary calibration error in the chopped signal, there will be an uncertainty in calibration during observing which depends on the signal bandwidth and the integration time. For a continuum calibration with Δt = 10 s,

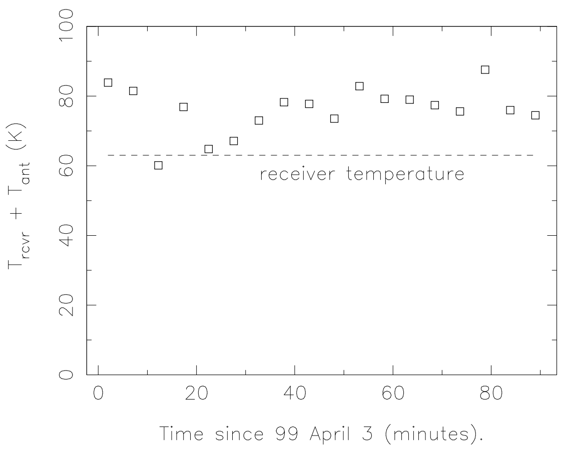

Figure 7. 225 GHz antenna temperature derived from linear fit to tipping curves.

$T_{sys(DSB)} = 200$ K, and $BW \simeq 1$ GHz, we find $\sigma_{\Delta T} = 4 \times 10^{-3}$ K, which is 0.2% of the calibration signal. The uncertainty is about 1% for a 20 MHz BW. Calibration of a narrower channel may be accomplished by a long calibration measurement made simultaneously with the interferometer phase calibration on a quasar.

5. Conclusions

We have succeeded in making a two-temperature radiometer calibration to 1%, with corresponding measurements of the atmospheric opacity. This should allow 1% amplitude calibration of observations made in good weather. During less-stable atmospheric conditions, the scheme may be used in the chopper wheel method, with the advantages of continuous measurements made at the receiver operating point and of an ambient load of well-known temperature. Characterization of the frequency response of the load coupling continues, and integration with observing procedures is underway in preparation for the installation of the new system on the remaining BIMA antennas.

Acknowledgments. This work was supported by the National Radio Astronomy Observatory through the Millimeter Development Consortium and by the NSF through grant AST 9413933.

References

Penzias, A. A. & Burrus, C. A. 1973, ARA&A, 11, 51